

Article

# Influence of a Surface Finishing Method on Light Collection Behaviour of PWO Scintillator Crystals

Daniele Rinaldi <sup>1</sup>, Luigi Montalto <sup>1</sup>, Michel Lebeau <sup>2,†</sup> and Paolo Mengucci <sup>1,\*</sup> 

<sup>1</sup> Dipartimento SIMAU, Università Politecnica delle Marche, 60131 Ancona, Italy; d.rinaldi@univpm.it (D.R.); l.montalto@univpm.it (L.M.)

<sup>2</sup> Former at PH Department CERN, 1211 Geneva 23, Switzerland; michel.lebeau@bluewin.ch

\* Correspondence: p.mengucci@univpm.it; Tel.: +39-071-2204733

† Retired.

Received: 7 October 2018; Accepted: 31 October 2018; Published: 4 November 2018



**Abstract:** In the field of scintillators, high scintillation and light production performance require high-quality crystals. Although the composition and structure of crystals are fundamental in this direction, their ultimate optical performance is strongly dependent on the surface finishing treatment. This paper compares two surface finishing methods in terms of the final structural condition of the surface and the relative light yield performances. The first polishing method is the conventional “Mechanical Diamond Polishing” (MDP) technique. The second polishing technique is a method applied in the electronics industry which is envisaged for finishing the surface treatment of scintillator crystals. This method, named “Chemical Mechanical Polishing” (CMP), is efficient in terms of the cost and material removal rate and is expected to produce low perturbed surface layers, with a possible improvement of the internal reflectivity and, in turn, the light collection efficiency. The two methods have been applied to a lead tungstate  $\text{PbWO}_4$  (PWO) single crystal due to the wide diffusion of this material in high energy physics (CERN, PANDA project) and diagnostic medical applications. The light yield (LY) values of both the MDP and CMP treated crystals were measured by using the facilities at CERN while their surface structure was investigated by Scanning Electron Microscopy (SEM) and Grazing Incidence X-ray Diffraction (GID). We present here the corresponding optical results and their relationship with the processing conditions and subsurface structure.

**Keywords:** scintillator crystals; polishing techniques; light yield; scanning electron microscopy; grazing incidence X-ray diffraction

## 1. Introduction

Applications in high energy physics, medicine, security, and environmental monitoring require more and more accurate and sensitive devices to accomplish new challenging goals. The high luminosity perspective of the Large Hadron Collider (LHC) [1] and the construction of the new PANDA detector [2] request great efforts in producing high-quality and homogeneous components for both accelerators and detectors [3]. In fact, the response of the electromagnetic calorimeters is critically determined by the performances of the scintillator crystals.

In nuclear medicine and bioimaging diagnostics, new frontiers are opened by fast, sensitive, and reliable devices and materials [4,5]. In this sense, the goal of 10 ps coincidence time resolution [6] will open a new era on the real-time diagnosis and monitoring of organs and body systems [7]. All these new trends request strong efforts in the production of new and high-quality scintillators. In order to face these challenges, the light performances of scintillator materials need to be improved through theoretical efforts and experimental assessment [8,9]. The condition of scintillators must be accurately evaluated, and it is mandatory to finely tune the production process parameters via feedback from

the crystal final state [10–12]. Structural conditions and elasto-optical properties of scintillators play a crucial role that must be deeply investigated [13,14]. The use of single crystals in electronics and high energy physics requires detailed knowledge of the structure of crystal surfaces and interfaces between different media, affecting signal propagation and transmission to transducers or light collection devices. Underestimating this factor may impair the whole system efficiency. In particular,  $\text{PbWO}_4$  (PWO) crystals, used in the complex experiment Compact Muon Solenoid (CMS) electromagnetic calorimeter and PANDA [1,2], require suitable, reliable and repeatable mechanical operations for cutting and polishing in order to guarantee the proper surface finishing state which influences the crystal optical properties such as light yield, optical transmission and energy resolution [15].

In the present work, two surface polishing techniques, namely Mechanical Diamond Polishing (MDP) and Chemical Mechanical Polishing (CMP) [16] are compared in terms of surface structure and optical performances of  $\text{PbWO}_4$  (PWO) crystals. The strong physical anisotropy of PWO crystals suggested their testing on two orthogonal sample orientations to evaluate the influence of the surface crystalline state in order to achieve the expected internal reflectivity by a reproducible finishing procedure. Recent works evidenced the necessity of high efficiency in the surface light reflection thus increasing the crystal light performances [17].

The surface structure of PWO crystals after polishing was investigated by Scanning Electron Microscopy (SEM) and Grazing Incidence X-ray Diffraction (GID), while Light Yield (LY) measurements were performed for optical properties determination [18]. Furthermore, GID analysis also allowed evaluating the thickness of the sub-surface layer damaged by each specific polishing treatment.

Although this work specifically addresses PWO scintillating crystals, the main results obtained can be considered for efficient surface processing in case of different materials and new applications.

## 2. Materials and Methods

### 2.1. Mechanical Diamond Polishing (MDP)

The outstanding hardness of diamond and the durability of the grains sharp edges result in a brittle fracture process and a high and regular material removal, opposed to the slower and stressing process of softer abrasives, mostly working by plastic deformation. With conventional lubricants, the processing energy increases by a factor 10 from diamond to softer abrasives (e.g., silicon carbide) [8]. Diamond polishing is the method chosen, for instance, by several PWO producers for finishing the CMS crystals.

### 2.2. Chemical Mechanical Polishing (CMP)

Several combinations of abrasives and chemical fluids have been developed under the term CMP. Colloidal silica is the best fit for the processing of dielectrics [6]. The specific chemical action of colloidal silica is due to its basic pH (9). The tiny silica grains, average size about 100 nm (Figure 1), in suspension are not likely to work by abrasion but tend to distribute the chemical action and avoid etching patterns.

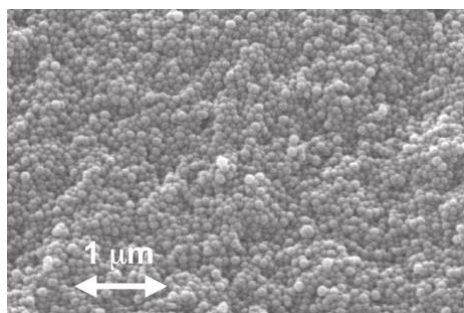


**Figure 1.** The Scanning Electron Microscopy (SEM) image of the colloidal silica abrasive grains, average size 100 nm.

### 2.3. Sample Selection and Preparation

Single crystals of lead tungsten oxide  $PbWO_4$  were prepared by the MDP and CMP techniques. In particular, all samples were initially submitted to the same MDP finishing treatment. Subsequently, only a set of samples among these were also submitted to the CMP finishing treatment. This latter set of samples are indicated from here on as CMP samples. Therefore, while the MDP samples had their surface finished by the MDP treatment only, the CMP samples were sequentially finished by the two treatments in the order MDP and CMP (details are reported below).

The sample size was chosen for meeting serial processing conditions. All surface treatments were performed on standard lapping and polishing machines with a serial production tooling (Figure 2).

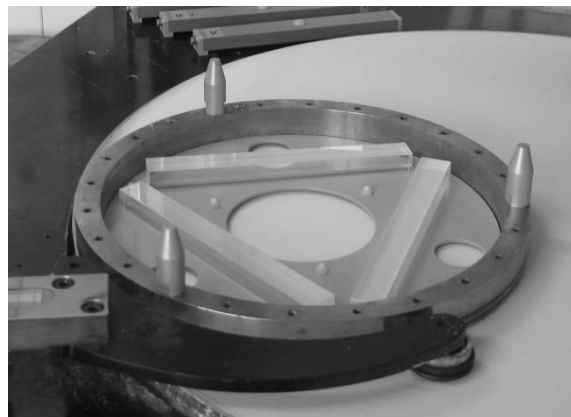


**Figure 2.** The sample mounting on the polishing tool used in commercially available polishing machines.

This tooling requires that the 3 crystals are processed at the same time. We selected as test crystal samples numbered 23,826, 32,134, and 32,138, from the CMS production series and close enough in shape to be processed together. The studied treatments were applied to the three-relevant side-faces: one of orientation [001], i.e., with c or optical axis normal to the face, and two faces of orientation [010], the fourth face being the matt face providing the uniformizing effect in CMS crystals (Figure 3).

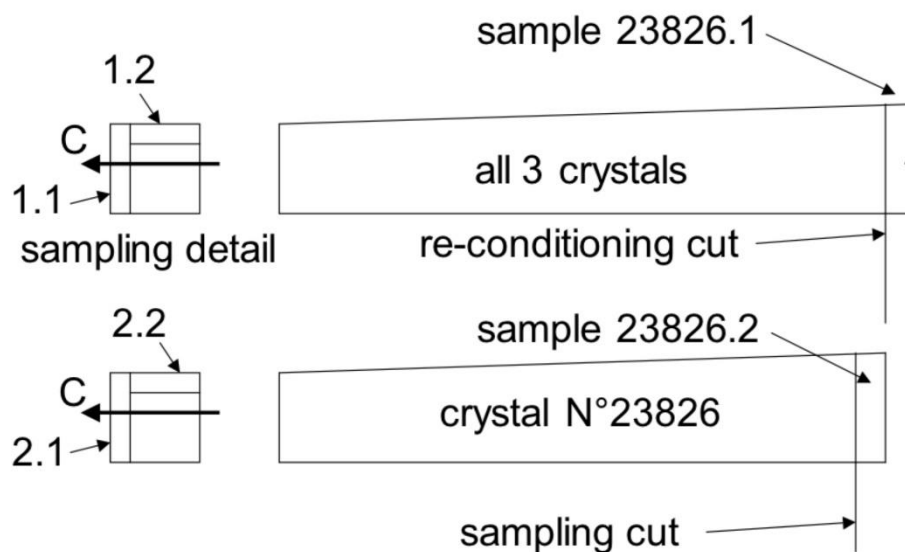


**Figure 3.** The schematics of the sampling map.

Treatment parameters are reported in Table 1, while the treatment sequence for obtaining samples of MDP and CMP finishes are detailed in Table 2.

**Table 1.** The surface treatment parameters.

<b>MDP Finishing</b>		
	<i>A—Original lapping</i>	<i>B—Mechanical diamond polishing</i>
abrasive	28 $\mu\text{m}$ corundum in water emulsion	2 $\mu\text{m}$ polycrystalline. diamond water emulsion
time-velocity-pressure	5 min - - manual	10 min-60 rpm-2N/cm <sup>2</sup>
removal [001]	50 $\mu\text{m}$ nominal	# 10 $\mu\text{m}$
removal [010]	50 $\mu\text{m}$ nominal	# 10 $\mu\text{m}$
<b>CMP Finishing</b>		
	<i>C—Re-conditioning lapping</i>	<i>D—Chemical mechanical polishing</i>
abrasive	15 $\mu\text{m}$ polycrystalline diamond water emulsion	colloidal silica in 50% water dilution
Time-velocity-pressure	10 min-60 rpm-2 N/cm <sup>2</sup>	10 min-60 rpm-2 N/cm <sup>2</sup>
removal [001]	40 $\mu\text{m}$ average	# 10 $\mu\text{m}$
removal [010]	68 $\mu\text{m}$ average	# 10 $\mu\text{m}$

**Table 2.** Treatment sequence.

<b>Treatment Sequence for MDP Finishing</b>		<b>Treatment Sequence for CMP Finishing</b>	
<b>Operation</b>	<b>Details</b>	<b>Operation</b>	<b>Details</b>
Starting state	conventional lapping (A) & polishing (B) of 3 side-faces	Lapping (C)	3 side-faces
Sampling 1 of crystal 1	Cutting 1.1 and.1.2	CMP (D)	3 side-faces
GID observations	Plots 1.1 and.1.2	Sampling 2 of crystal 1	Cutting 2.1 and 2.2
Optical measurement	Crystals 2 & 3	GID observations	Plots 2.1 and 2.2

One 5 mm-thick slice was cut-off from sample n. 23,826 large end at each step, and  $20 \times 10 \times 5 \text{ mm}^3$  parallelepipeds cut from each slice to present an original  $20 \times 10 \text{ mm}^2$  area for GID observations (Figure 3). Crystals n. 32,134 and n. 32,138 were kept to 220 mm length throughout the sequence for the study of the scintillating light yield.

#### 2.4. Grazing Incidence X-ray Diffraction (GID)

Grazing incidence X-ray diffraction (GID) was carried out by an INEL CPS 120 diffractometer equipped with a computerized goniometer using the Cu-K $\alpha$  radiation. Four different incidence angles ( $0.4^\circ$ ,  $1^\circ$ ,  $2^\circ$  and  $4^\circ$ ) were used in order to study the structure variation as a function of depth below the sample surface. Two different sample orientations were investigated: (a) samples oriented in [001] and (b) samples oriented in [010] direction. Because of the tetragonal symmetry notations [010] and [100] are equivalent and we have omitted the sign notation as irrelevant in this work. The crystal growth direction used for the sample reference may differ from the lattice direction by less than  $5^\circ$ . For each orientation, we have analyzed samples with the MDP (#1.1 and #1.2) and CMP (#2.1 and #2.2) surface finishing treatments.

#### 2.5. Light Yield (LY) Measurements

Light yield measurements were performed at CERN, PH-CMX group by using an experimental set-up equipped with a Photo Multiplier Tube Photonis XP2020Q (Photonis s.a.s, Brive, France) and a Caen Digitizer (CAEN Technologies, Inc., NY, USA. A Cesium-137 source (CERN, Geneve, Switzerland) was used to characterize crystals that were optically coupled with optical grease to the photocathode and fully wrapped in Teflon. The quantum efficiency of the crystals was obtained by convolution of

the emission spectrum of crystals with the quantum efficiency of the tube. The LY was calculated after estimation of the peak position by deconvolution of the full energy spectrum; the results are provided in photoelectrons/MeV (p.e./MeV). Furthermore, LY measurements allowed obtaining the front (FNUF) and rear (RNUF) non-uniformity, defined as the slope of a linear fit performed over the LY distribution as a function of the source position along the crystal axis from 3.5 mm to 11.5 mm from the front and rear crystal faces, respectively.

### 3. Results

#### 3.1. GID

The results obtained by the GID analysis performed on the different samples are reported in Figure 4.

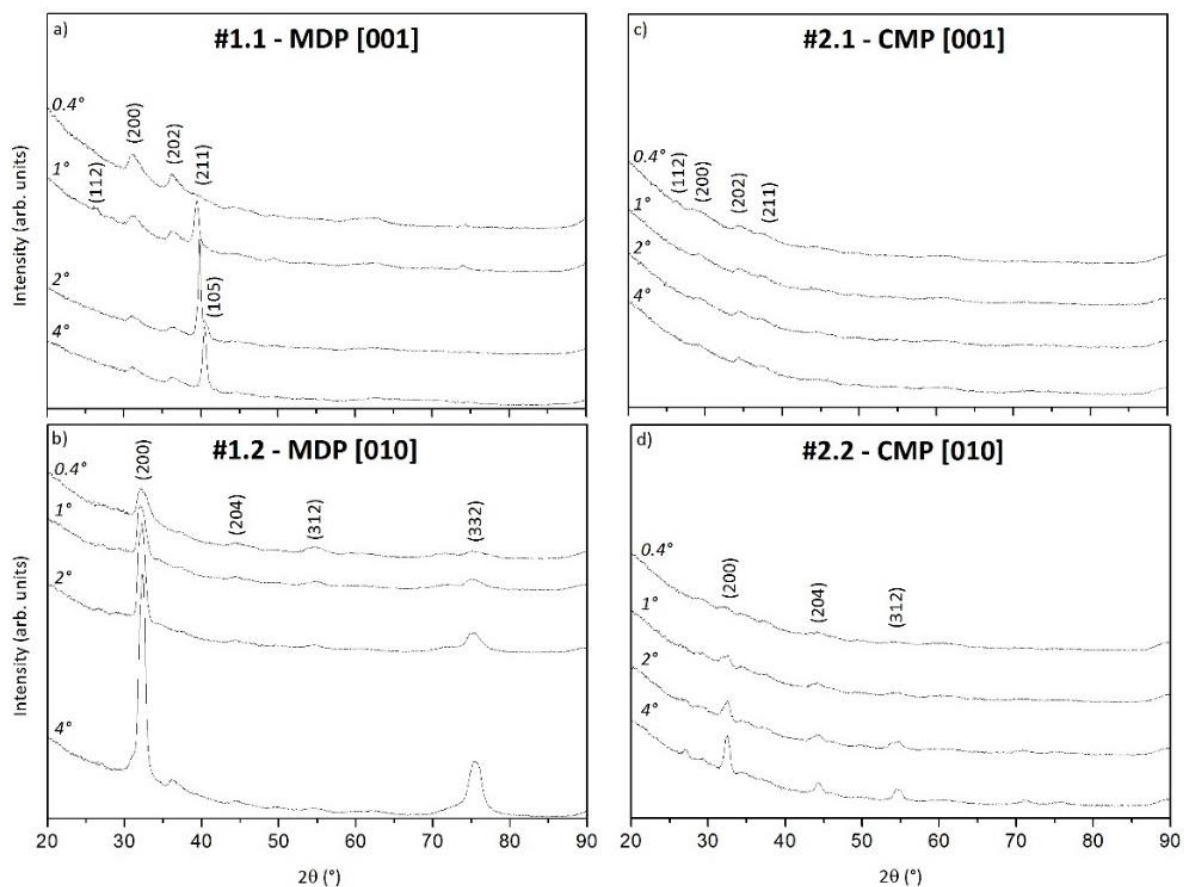


**Figure 4.** The Grazing Incidence X-ray Diffraction (GID) patterns of the Mechanical Diamond Polishing (MDP) and Chemical Mechanical Polishing (CMP) samples taken at four incidence angles ( $0.4^\circ$ ,  $1^\circ$ ,  $2^\circ$ , and  $4^\circ$ ) on the two different crystal orientations: (a) MDP [001], (b) MDP [010], (c) CMP [001], (d) CMP [010].

Peaks are due to the  $\text{PbWO}_4$  (Stolzite) compound with a tetragonal structure with lattice parameters  $a = b = 0.54619$  nm and  $c = 1.2049$  nm (ICDD file n. 19-708). All patterns are reported at the same scale in each figure and the main peaks visible are indexed by the corresponding Miller indices. Figure 4a refers to the MDP sample with the  $c$  axis perpendicular to the sample surface ([001] orientation) whereas Figure 4b reports the GID patterns of the same sample oriented with the  $c$  axis parallel to the sample surface ([010] orientation). It is worth noting that only a few peaks are visible and that their intensity varies with the incidence angle. This is a typical effect of the GID asymmetrical geometry which allows us to obtain information only from lattice planes inclined to the sample surface.

As an example, comparing patterns reported in Figure 4a,b, one may note that the main peak visible in sample #1.1 (MDP [001]) is (211) while that in sample #1.2 (MDP [010]) is (200), in agreement with the different surface orientation of the two samples. Furthermore, considering the relative intensity of peaks in the GID patterns of the MDP samples (Figure 4a,b), it is evident that (a) the crystalline structure of samples is retained from the top surface (patterns at  $0.4^\circ$ ) and tends to improve with depth (patterns at  $1^\circ$ ,  $2^\circ$  and  $4^\circ$ ), (b) the top surface of the MDP [010] sample is better crystallized with respect to the MDP [001] one. This latter observation suggests that the thickness of the surface amorphous layer produced by the MDP polishing treatment depends on the surface orientation, being lower for the [010] direction than the [001] one.

After the CMP treatment, GID patterns (Figure 4c,d) clearly differ from the previous ones. In particular, the peak intensity is strongly reduced for both orientations. While small residual peaks appear for the #2.2—CMP [010] sample (Figure 4d), patterns of the #2.1—CMP [001] sample do not present any evident peak (Figure 4c), looking like typical spectra of poorly crystallized material. For the #2.2—CMP [010] sample (Figure 4d) only the pattern at  $0.4^\circ$  of incidence does not present any evident peak, while at  $1^\circ$ , a weak (200) peak is visible. Considering that the total thickness analyzed by GID is about  $0.05\ \mu\text{m}$  at an incidence angle of  $0.4^\circ$ , about  $0.1\ \mu\text{m}$  at  $1^\circ$ , and about  $0.3\ \mu\text{m}$  at  $4^\circ$ , one can conclude that the CMP treatment produces an amorphous surface layer whose thickness depends on the face orientation. In the [001] orientation the CMP-induced surface amorphous layer extends at least down to  $0.3\ \mu\text{m}$  (Figure 4c). In the [010] orientation its thickness ranges between  $0.05\ \mu\text{m}$  and  $0.1\ \mu\text{m}$  (Figure 4d).

These results allow us to conclude that the CMP treatment produces a thicker surface amorphous layer than the MDP one. Furthermore, both MDP and CMP treatments, although suitable for producing a fine surface finish, tend to produce an amorphous surface layer whose thickness depends on the lattice orientation. This amorphous surface layer is thicker on the surface normal to the c axis ([001] orientation).

### 3.2. Surface Finish and Micro-Geometry

Comparing the microscopic observations (Figure 5) of crystals with MDP (Figure 5a) and CMP (Figure 5b) surface finish at similar locations on the crystal face and with same lattice orientations show that the dense network of fine scratches of the MDP finish has disappeared with the CMP finish.

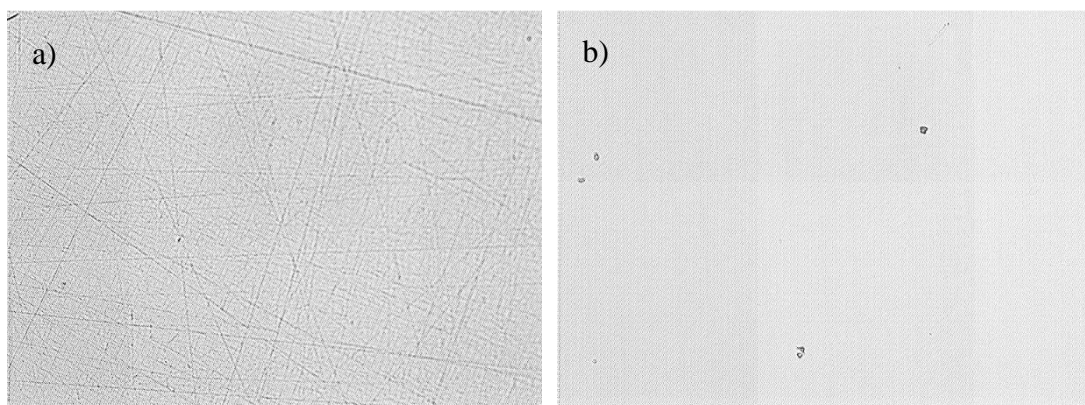


**Figure 5.** The optical microscopy images of the samples: (a) MDP [001], (b) CMP [001]. Magnification =  $200\times$ .

Roughness measurements for the MDP treated surface range from 6 to 30 nm Ra (average roughness), corresponding to 40 to 180 nm Rt or peak-to-valley, compatible with the visual aspect required by the CMS specification, whereas CMP ranges from 2 to 5 nm Ra (12 to 30 nm Rt).

### 3.3. Light Yield (LY)

After the three crystals received identical treatments (Figure 2), crystals N°32134 and N°32138 were placed on an optical bench [18] for light yield (LY) measurements whereas crystal N°23826 was sampled (Figure 3) for GID observations. Optical results are reported in Table 3 where light yield (LY), front non-uniformity (FNUF) and rear non-uniformity (RNUF) [17] are listed for the two samples submitted to MDP and CMP surface finishing. All values in Table 3 are reported with the corresponding standard deviation. LY results in Table 3 show an improvement of the surface finishing state from the MDP to the CMP treatment of +1% (sample #38138) and +2% (sample #32134), respectively, for the two measured crystals.

**Table 3.** The optical results obtained from measurements on samples submitted to the Mechanical Diamond Polishing (MDP) and Chemical Mechanical Polishing (CMP) surface finishing. Average values and corresponding standard deviation ( $\sigma$ ) are reported. LY = Light Yield, FNUF = Front Non-UniFormity, RNUF = Rear Non-UniFormity.

Sample	Treatment	LY (p.e./MeV)		FNUF (%/X <sub>0</sub> )		RNUF (%/X <sub>0</sub> )	
		Average	$\sigma$	Average	$\sigma$	Average	$\sigma$
#38138	MDP	12.18	0.07	0.020	0.023	−0.056	0.046
	CMP	12.28	0.06	−0.180	0.020	−0.012	0.040
#32134	MDP	13.40	0.13	0.032	0.040	0.077	0.080
	CMP	13.69	0.07	−0.076	0.020	0.115	0.040

It is worth to note that Diehl et al. [19] have investigated the influence of surface roughness on the LY response of PWO crystals of the PANDA detector. In particular, they found variations in the LY response for the crystal surface with an average roughness  $R_a = 0.3 \mu\text{m}$ . In our case, the surface roughness of the MDP and CMP treated samples is always much lower than the value reported by Diehl et al. [19]. Therefore, one can conclude that the scattering effects of the incident excitation radiation due to surface roughness in both MDP and CMP samples have negligible influence on the LY results.

The LY increment is significant, especially when cumulative effects take place as is the case of an entire detection system which requires a contribution from the different parts to reduce uncertainty and enhance sensitivity, reliability, and accuracy.

## 4. Discussion

The initial intention for applying CMP was for removing an assumed damaged surface layer from lapping, thanks to the apparently smoother processing conditions. GID results show, however, that after MDP diamond polishing, the potential damage of lapping treatment is undetected. This confirms that which was in the abundant literature describing the work by the brittle fracture of diamond processing in contrast to the work by plastic deformation of softer abrasives [20–22]. On the other hand, GID shows that CMP produces an amorphous layer, the thickness of which is out of scale with and cannot be caused by the previous lapping. We attribute this thin amorphous layer to the combined action of the chemical and mechanical removal of the material from the crystal surface during the CMP treatment.

The different thickness layers reflect the material anisotropy in terms of workability as shown by the lapping removal rate difference (Table 1, Treatment C). CMP performs an efficient material removal of about  $1 \mu\text{m}/\text{min}$ , comparable to conventional diamond polishing ( $2 \mu\text{m}$  grit) without a noticeable processing forces increase.

The amorphous-like layer thickness in CMP is higher than  $0.3 \mu\text{m}$  for the [001] direction, about  $3/4$  of the scintillating light wavelength  $\lambda = 425 \text{ nm}$  [23,24]. If the refractive index of the

amorphous phase differs from the crystalline phase index, the thickness of the polished part is sufficient to avoid any possible optical tunneling effects due to the match of different refractive layers [25]. This results in an internal reflection of light that reduces the light transmission out of the crystal volume. The net improvement in the surface finish by a factor 3 to 6 in Ra strongly contributes to the LY improvement. Therefore, the smoother CMP surface enhances the total internal reflection effect.

On the contrary, the high density of scratches in the MDP finished surface creates easy paths for light to escape from the crystal volume. Light diffused out of the crystal cannot reach the photomultiplier, thus, decreasing the crystal optical performance. In other words, due to the presence of scratches on the crystal surface, light interacting with the inner crystal surface is no more in a critical angle condition over the sample surface [25].

The considerations reported above also give reason to the net improvement of the FNUF of the CMP finished sample. The enhanced internal reflectivity improves the focusing effect on the front side of the crystal (Table 3). On the contrary, no relevant benefits come from the CMP polishing for the RNUF (Table 3) [17]. In this case, although the crystal surface is acting as a reflector, the absorption phenomena become predominant in this area of the sample.

Currently, research in this direction is not sufficiently developed, further efforts should be focused on the correlation between optical anisotropies and local refraction index variations.

## 5. Conclusions

Consumption tests performed in realistic conditions showed that polishing with diamond costs about 3 times more than CMP. To obtain the same finish as with CMP (2 to 5 nm Ra) with diamond, a second polishing step with finer diamond grain would be necessary, and a cost factor of 5 to 6 was reached, not to mention the additional tooling and processing time. Furthermore, it is evident that, without specific tuning and using commercial products, CMP produced some improvement in the scintillating crystal light yield and FNUF. This shows an economical direction for increasing the optical output thanks to an optimization of light collection and surface finish. GID has proven to be a very convenient and accurate method for the surface qualitative and quantitative evaluation adapted for this research.

**Author Contributions:** Conceptualization, D.R. and M.L.; Data curation, L.M.; Investigation, D.R., M.L. and P.M.; Methodology, D.R., M.L. and P.M.; Writing—original draft, D.R., M.L. and P.M.; Writing—review & editing, L.M. and P.M.

**Funding:** This research received no external funding.

**Acknowledgments:** This research paper is in the framework of the Crystal Clear Collaboration (CERN), the PANDA project at Darmstadt and the COST Action TD1401 (FAST).

**Conflicts of Interest:** The authors declare no conflict of interest.

## References

1. Arduini, G.; Barranco, J.; Bertarelli, A.; Van der Veken, F.; Biancacci, N.; Bruce, R.; Brüning, O.; Buffat, X.; Cai, Y.; Carver, L.R.; et al. High Luminosity LHC: Challenges and plans. *J. Instrum.* **2016**, *11*, C12081. [[CrossRef](#)]
2. Andersson, W.I. The PANDA Detector at FAIR. *J. Phys.* **2016**, *770*, 012043. [[CrossRef](#)]
3. Apollinari, G.; Béjar Alonso, I.; Brüning, O.; Lamont, M.; Rossi, L. High-Luminosity Large Hadron Collider (HL-LHC). In *Preliminary Design Report*; CERN: Geneva, Switzerland, 2015.
4. David, S.; Georgiou, M.; Fysikopoulos, E.; Belcari, N.; Loudos, G. Imaging performance of silicon photomultipliers coupled to BGO and CsI:Na arrays. *J. Instrum.* **2013**, *8*, 12008. [[CrossRef](#)]
5. David, S.; Georgiou, M.; Fysikopoulos, E.; Loudos, G. Evaluation of a SiPM array coupled to a Gd<sub>3</sub>Al<sub>2</sub>Ga<sub>3</sub>O<sub>12</sub>:Ce (GAGG:Ce) discrete scintillator. *Phys. Med.* **2015**, *31*, 763–766. [[CrossRef](#)] [[PubMed](#)]
6. Lecoq, P. Pushing the Limits in Time-of-Flight PET Imaging. *IEEE Trans. Radiat. Plasma Med. Sci.* **2017**, *1*, 473–485. [[CrossRef](#)]

7. Cherry, S.R.; Jones, T.; Karp, J.S.; Qi, J.; Moses, W.W.; Badawi, R.D. Total-Body PET: Maximizing Sensitivity to Create New Opportunities for Clinical Research and Patient Care. *J. Nucl. Med.* **2018**, *59*, 3–12. [[CrossRef](#)] [[PubMed](#)]
8. Mengucci, P.; Di Cristoforo, A.; Lebeau, M.; Majni, G.; Paone, N.; Pietroni, P.; Rinaldi, D. Surface quality inspection of PbWO<sub>4</sub> crystals by grazing incidence X-ray diffraction. *Nucl. Instrum. Methods Phys. Res. A* **2005**, *537*, 207–210. [[CrossRef](#)]
9. Mengucci, P.; André, G.; Auffray, E.; Barucca, G.; Cecchi, C.; Chipaux, R.; Cousson, A.; Davì, F.; Di Vara, N.; Rinaldi, D.; et al. Structural, Mechanical and Light Yield Characterisation of Heat Treated LYSO:Ce Single Crystals for Medical Imaging Applications. *Nucl. Instrum. Methods Phys. Res. A* **2015**, *785*, 110–116. [[CrossRef](#)]
10. Montalto, L.; Natali, P.P.; Davì, F.; Mengucci, P.; Paone, N.; Rinaldi, D. Characterization of a Defective PbWO<sub>4</sub> Crystal Cut Along the a-c Crystallographic Plane: Structural Assessment and a Novel Photoelastic Stress Analysis. *J. Instrum.* **2017**, *12*, 12035. [[CrossRef](#)]
11. Natali, P.P.; Montalto, L.; Davì, F.; Mengucci, P.; Ciriaco, A.; Paone, N.; Rinaldi, D. Theoretical and Experimental Evaluation of Piezo-Optic Parameters and Photoelastic Constant in Tetragonal PWO. *Appl. Opt.* **2018**, *57*, 730–737. [[CrossRef](#)] [[PubMed](#)]
12. Montalto, L.; Rinaldi, D.; Paone, N.; Scalise, L.; Davì, F. Photoelastic Sphenoscopic Analysis of Crystals. *Rev. Sci. Instrum.* **2016**, *87*, 015113. [[CrossRef](#)] [[PubMed](#)]
13. Davì, F.; Rinaldi, D. Mechanical and Optical Properties of Anisotropic Single-Crystal Prisms. *J. Elast.* **2015**, *120*, 197–224. [[CrossRef](#)]
14. Rinaldi, D.; Davì, F.; Montalto, L. On the Photoelastic Constants and the Brewster Law for Stressed Tetragonal Crystals. *Math. Methods Appl. Sci.* **2018**, *41*, 3103–3116. [[CrossRef](#)]
15. Mao, R.; Zhang, L.; Zhu, R.Y. Optical and Scintillation Properties of Inorganic Scintillators in High Energy Physics. *IEEE Trans. Nucl. Sci.* **2008**, *55*, 2425–2431. [[CrossRef](#)]
16. Vlassak, J.J. A Model for Chemical–Mechanical Polishing of a Material Surface Based on Contact Mechanics. *J. Mech. Phys. Solids* **2004**, *52*, 847–873. [[CrossRef](#)]
17. Diehl, S.; Brinkmann, K.T.; Drexler, P.; Dormenev, V.; Novotny, R.W.; Rosenbaum, C.; Zaunick, H.G. Impact of Non-Uniformity in Light Collection on the Energy Resolution of the PANDA Electromagnetic Calorimeter at Photon Energies Below 1 GeV. *J. Phys.* **2017**, *928*, 012040. [[CrossRef](#)]
18. Borgia, B.; Baccaro, S. *Tungstate Crystals: Proceedings of the International Workshop on Tungstate Crystals*; Università degli studi La Sapienza: Rome, Italy, 1999; ISBN 8887242100.
19. Diehl, S.; Bremer, D.; Brinkmann, K.T.; Dormenev, V.; Eissner, T.; Novotny, R.W.; Rosenbaum, C.; Zaunick, H.G. Measurements and Optimization of the Light Collection Uniformity in Strongly Tapered PWO Crystals of the PANDA Detector. *Nucl. Instrum. Methods Phys. Res. A* **2017**, *857*, 1–6. [[CrossRef](#)]
20. Wapler, W.; Juchem, H.O. Diamond abrasive for Machining glass. *Ind. Diam. Rev.* **1987**, *4*, 159–162.
21. Huerta, M.; Malkin, S. Grinding of Glass: The Mechanics of the Process. *J. Eng. Ind.* **1976**, 459–467. [[CrossRef](#)]
22. Malkin, S.; Ritter, J.E. Grinding Mechanisms and Strength Degradation for Ceramics. *J. Eng. Ind.* **1989**, *111*, 167–174. [[CrossRef](#)]
23. Senguttuvan, N.; Ishii, M.; Tanji, K.; Kittaka, T.; Usuki, Y.; Kobayashi, M.; Nikl, M. Influence of Annealing on the Optical Properties of PbWO<sub>4</sub> Single Crystals Grown by the Bridgman Method. *Jpn. J. Appl. Phys.* **2000**, *39*, 5134. [[CrossRef](#)]
24. Mao, R.; Zhang, L.; Zhu, R.Y. Quality of Mass-Produced Lead Tungstate Crystals. In Proceedings of the 2003 IEEE Nuclear Science Symposium, Conference Record (IEEE Cat. No.03CH37515), Portland, OR, USA, 19–25 October 2003. [[CrossRef](#)]
25. Kasap, S.O. *Optoelectronics and Photonics: Principles and Practices*, 2nd ed.; University of Saskatchewan: Saskatoon, SK, Canada; Pearson: London, UK, 2013; ISBN-13 9780201610871.

